

Estimation of Radiation Source Distribution Using Structure Information for Fukushima Daiichi Nuclear Power Plant Reactor

Ziheng Chao¹, Ren Komatsu¹, Hanwool Woo¹, Yusuke Tamura², Atsushi Yamashita¹, and Hajime Asama¹

Abstract— This study proposes a highly accurate method for estimating the distribution of radiation sources, using a particle filter of the Bayesian estimation framework, which incorporates the structural information of the reactor at the Fukushima Daiichi Nuclear Power Plant as the prior information. From the experimental result, unlike the maximum likelihood estimation method, our method performed well in an extreme measurement environment where the detector could not reach, and showed high accuracy in the estimation of the point-like and the distributed radiation sources.

I. INTRODUCTION

A. Background

Distribution estimation for radioactive materials has been widely conducted for disaster rescue and prevention. Particularly, the 2011 Fukushima Daiichi nuclear disaster attracted worldwide attention. The situation at Fukushima Daiichi Nuclear Power Plant after the disaster has been systematically investigated [1], and some conditions, such as internal information of the reactor, are becoming more apparent. As shown in Fig. 1, numerous nuclear fuels initially present in the pressure vessel (RPV) of reactor Unit 2 melted through the platform, which is the upper structure of the pedestal of the primary containment vessel (PCV), during the Fukushima Daiichi nuclear disaster, creating holes in the platform and falling through the holes to the bottom of the pedestal, generating debris. Figure 2 shows the actual structure [2], the part surrounded by the red line in the lower part of Fig. 2 is the hole created by debris. Based on the environment and safety of residents, it is necessary to remove debris. As the pre-process of removal work, it is important to estimate the distribution of radioactive materials at the bottom of the pedestal, especially radiation sources likely located below the hole in the structure.

Before estimating the distribution of radioactive materials, the radiation detector is often used in the investigation of radioactive materials to measure the radiation dose rate. In the current situation of the Fukushima Daiichi Nuclear Power Plant Unit 2, because it is unrealistic for the operator to measure the radiation inside the pedestal actually, unmanned measurements are required. The proposed concept is shown in Fig. 1, install the radiation detector in a robot arm mechanism, and extend the robot arm to the pedestal from the platform. To maintain the stability of the mechanism, a large load should be applied to the structure, which limits

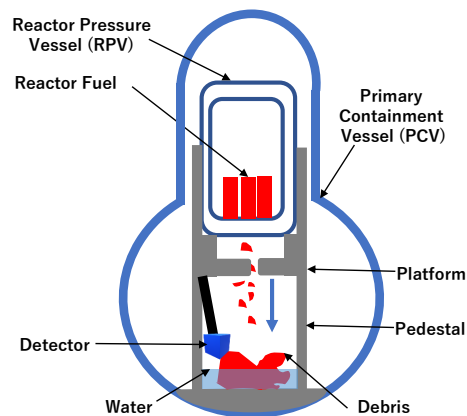


Fig. 1. Schematic diagram of nuclear reactor Unit 2



Fig. 2. Actual situation of the structure above the pedestal [2], to clearly show the location and state of the hole, we modified the figure by circling the hole at the bottom of the diagram with a red line.

the operating range of the robot arm, and the primary movement is in the vertical direction rather than in the horizontal direction. However, the reactor is in a highly complex environment, and the internal structure is disrupted by the nuclear fuel. This complicated environment posed a significant challenge to the survey of radiation sources in the pedestal, especially in areas where detectors could not reach. As shown in Fig. 3, which is the schematic top-view of the pedestal, there is an area called the undetectable area where the robot arm, which does not have a superior performance in the horizontal operation, cannot actually reach. Particularly, part of the area directly under the holes created by accident, is an undetectable area. Therefore, the estimation of radiation sources in the undetectable area is an important issue. In recent years, information about inside Fukushima reactors has been clarified, and [3] recreated the situation in which fuel debris, including radioactive materials, goes through

¹Department of Precision Engineering, University of Tokyo, Hongo 7-3-1, Bunkyo, Tokyo, Japan

²Department of Robotics, Tohoku University, 6-6-01, Aramaki Aza Aoba, Aoba-ku, Sendai, Miyagi, Japan

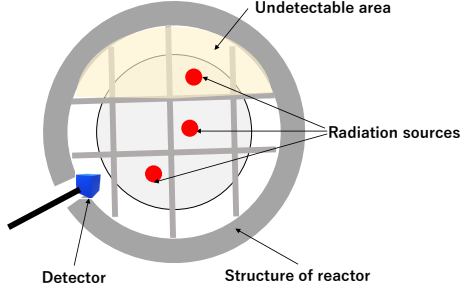


Fig. 3. Undetectable area inside the pedestal

the holes and falls. This reveals that even if the detector cannot reach directly under the hole, it can effectively use the information about the probable existence of radiation sources directly under the hole and the information about the hole in the platform, as prior information for distribution estimation of radiation sources.

B. Related Work

Numerous studies on radiation source distribution estimation have been conducted to detect radiation intensity using two main approaches: directional or non-directional detector. Several studies have used directional detectors, such as Compton cameras [4], TimePix [5], and gamma cameras [6], which can obtain the energy of the radiation and its incidence angle to estimate the radiation source distribution. However, it is difficult to use a directional detector in a high dose rate environment comprising numerous radiation sources, such as the Fukushima Daiichi Nuclear Power Plant. Therefore, using a non-directional detector is more practical, which can only obtain energy information, such as the dose rate and count number. Some studies have revealed that non-directional detectors can efficiently estimate the radiation source distribution [7], [8], [9], [10], [11], [12]. In [7], multi-resolution grid computation and maximum likelihood estimation (MLE) were merged to quickly localize the radiation source. In [11], the MLE and Bayesian methods were compared. Grid-based MLE divides the area into several grids where radiation is likely to exist, called the region of interest (ROI), places detectors at a lot of measurement spots at ROI, and estimates the value of each grid group based on the obtained radiation counts. The dose distribution determines the upper limit of the estimation performance, because this method uses only the radiation dose distribution. Therefore, it does not cope well with the situation where there are undetectable areas.

In addition to using dose information, it is helpful to use prior information, such as the structure information of the hole above the undetectable area, as stated in Section I-A. In this study, we propose a method for accurate radiation source distribution estimation, even in the presence of undetectable areas, by using prior information. In addition to the incorporation of prior information, we also contribute to formulating models for two types of radiation sources: point-like radiation sources and distributed radiation sources.

II. RADIATION SOURCE DISTRIBUTION BAYESIAN ESTIMATION FRAMEWORK

A. Mathematical Model of Radiation Sources and Detectors

1) *Point-like Radiation Source*: The point-like radiation source is the simplest case, and when the actual volume of the radiation source is relatively small, it is convenient and effective to treat it as a point-like radiation source. We set $\mathbf{q} = [\mathbf{q}_1, \mathbf{q}_2, \dots, \mathbf{q}_i, \dots, \mathbf{q}_N]^T$, which is the set of radiation sources, where $\mathbf{q}_i = [\mathbf{x}^{\mathbf{q}_i}, \pi_i]^T \in \mathbb{R}^3 \times \mathbb{R}^+$, $i = [1, 2, \dots, N]$, $\mathbf{x}^{\mathbf{q}_i}$ as the location, and π_i is the intensity of the i th radiation source. Further, we set $\mathbf{b} = [\mathbf{b}_1, \mathbf{b}_2, \dots, \mathbf{b}_M]^T$, as the count numbers obtained by detectors at M measurement spots, where $\mathbf{b}_i = [\mathbf{x}^{\mathbf{b}_i}, m_i]^T \in \mathbb{R}^3 \times \mathbb{R}^+$, $i = [1, 2, \dots, M]$, $\mathbf{x}^{\mathbf{b}_i}$ is the location of the i th measurement spot, and m_i is the value of count number. In the measurement of radiation sources, because the measurements and radiation sources follow the inverse square law, the relationship between m_i , which is the measurement at spot i to all radiation sources \mathbf{q} , can be expressed as follows:

$$m_i(\mathbf{q}) = \sum_j^N \frac{c\pi_j}{\|\mathbf{x}^{\mathbf{b}_i} - \mathbf{x}^{\mathbf{q}_j}\|^2} e^{-\mu t}. \quad (1)$$

Notably, c is the coefficient of the detector, and μ is the radiation attenuation coefficient.

2) *Distributed Radiation Source*: The distributed radiation source has a certain area and cannot be easily applied to the point-like source model introduced in Section II-A.1. It is possible to consider a distributed radiation source that consists of many point-like sources by using Eq. (1), but in the estimation process, there is a risk that an ill-posed problem may occur. Therefore, a computational difficulty should be minimized and build a more efficient model. Here, we used the grid-based model introduced in [11], [13] to build the model.

We set $\mathbf{q}_i = [\mathbf{q}^{c_i}, \mathbf{q}^{w_i}, q^{t_i}]^T \in \mathbb{R}^3 \times \mathbb{R}^3 \times \mathbb{R}^+$, where \mathbf{q}^{c_i} is the central point, \mathbf{q}^{w_i} is the width, and q^{t_i} is the overall intensity of the No. i distributed radiation source. Then, based on \mathbf{q}^{c_i} and \mathbf{q}^{w_i} , we generated $\mathbf{g}_i = [\mathbf{x}^{\mathbf{g}_i}, \mathbf{q}^{\mathbf{g}_i}]^T \in \mathbb{R}^3 \times \mathbb{R}^+$ of S equal-sized grids in the area. Here, $\mathbf{x}^{\mathbf{g}_i}$ is the known location of all grids, and $\mathbf{q}^{\mathbf{g}_i}$ is the intensity of each grid. If we assume that \mathbf{q}_i follows a certain distribution, the probability density function \mathcal{P}_i can be generated. We set $\mathbf{q}^{\mathbf{g}_i} = \mathcal{P}_i(q^{t_i})$. The relationship between the measurement m_i and grid intensity $\mathbf{q}^{\mathbf{g}_i}$ can be written as follows:

$$m_i(\mathbf{q}) = \sum_j^N \sum_k^S \frac{c\mathbf{q}^{\mathbf{g}_{jk}}}{\|\mathbf{x}^{\mathbf{b}_i} - \mathbf{x}^{\mathbf{g}_{jk}}\|^2} e^{-\mu t}. \quad (2)$$

B. Estimation Model and Optimization Process

The Bayesian estimation framework estimates the posterior probability with radiation sources as a variable, and the posterior probability can be written as follows:

$$p(\mathbf{q}|\mathbf{b}) = \frac{p(\mathbf{b}|\mathbf{q})p(\mathbf{q})}{\int p(\mathbf{b}|\mathbf{q})p(\mathbf{q})d\mathbf{q}}. \quad (3)$$

From Eq. (3), it is difficult to calculate the integral equation of the denominator accurately, and the particle filter is a typical approach to solve this problem. First, the prior distribution $p(\mathbf{q})$ can be represented by N particles by approximating it with the following Dirac delta function:

$$p(\mathbf{q}) = \frac{1}{N} \sum_k^N \delta(\mathbf{q} - \mathbf{q}^k). \quad (4)$$

Next, we substitute the prior distribution in Eq. (3) and write the posterior probabilities as follows:

$$\begin{aligned} p(\mathbf{q}|\mathbf{b}) &= \frac{p(\mathbf{b}|\mathbf{q}) \frac{1}{N} \sum_{k=1}^N \delta(\mathbf{q} - \mathbf{q}^k)}{\int p(\mathbf{b}|\mathbf{q}) \frac{1}{N} \sum_{k=1}^N \delta(\mathbf{q} - \mathbf{q}^k)} \\ &= \frac{\sum_{k=1}^N p(\mathbf{b}|\mathbf{q}^k) \delta(\mathbf{q} - \mathbf{q}^k)}{\sum_{k=1}^N p(\mathbf{b}|\mathbf{q}^k)} \\ &= \sum_{k=1}^N \frac{p(\mathbf{b}|\mathbf{q}^k) \delta(\mathbf{q} - \mathbf{q}^k)}{\sum_{k=1}^N p(\mathbf{b}|\mathbf{q}^k)}. \end{aligned} \quad (5)$$

The count numbers measured at each spot of the detector were regarded as independent values, and the likelihood function $p(\mathbf{b}|\mathbf{q})$ is given by the following equation:

$$p(\mathbf{b}|\mathbf{q}) = p(\mathbf{b}_1|\mathbf{q})p(\mathbf{b}_2|\mathbf{q}) \cdots p(\mathbf{b}_i|\mathbf{q}) \cdots p(\mathbf{b}_n|\mathbf{q}). \quad (6)$$

Because the count numbers measured by the detector were known to follow the Poisson distribution, each probability $p(\mathbf{b}_i|\mathbf{q})$ that independently occurred is given by the following equation:

$$p(\mathbf{b}_i|\mathbf{q}) = \frac{(m_i(\mathbf{q}))^{m_i} e^{-m_i(\mathbf{q})}}{m_i!}. \quad (7)$$

According to Eq. (6), the likelihood function $p(\mathbf{b}|\mathbf{q})$ can be written as follows:

$$p(\mathbf{b}|\mathbf{q}) = \prod_{i=1}^M \frac{(m_i(\mathbf{q}))^{m_i} e^{-m_i(\mathbf{q})}}{m_i!}. \quad (8)$$

To incorporate the likelihood function more easily, it is convenient to take the logarithm of $p(\mathbf{b}|\mathbf{q})$:

$$\begin{aligned} p(\mathbf{b}|\mathbf{q}) &= \log p(\mathbf{b}|\mathbf{q}) \\ &= \log \prod_{i=1}^M \frac{1}{m_i!} + \log \prod_{i=1}^M (m_i(\mathbf{q}))^{m_i} e^{-m_i(\mathbf{q})}. \end{aligned} \quad (9)$$

Because the first term in Eq. (9) is constant, we should only consider the second term, while the second term is given by the following equation:

$$\log \prod_{i=1}^M (m_i(\mathbf{q}))^{m_i} e^{-m_i(\mathbf{q})} = \sum_{i=1}^M m_i \log m_i(\mathbf{q}) - \sum_{i=1}^M m_i(\mathbf{q}). \quad (10)$$

Here, the weight of each particle can be written by normalizing the likelihood function using the following equation:

$$\mathbf{w}^k = \frac{p(\mathbf{b}|\mathbf{q}^k)}{\sum_{k=1}^N p(\mathbf{b}|\mathbf{q}^k)}. \quad (11)$$

Algorithm 1 Radiation source distribution estimation using particle filter

- 1: Scatter N particles $\mathbf{Q}_{0|0}$ ▷ Prior information
 - 2: **for** t in $(1, \dots, T)$ epoch **do**
 - 3: **for** i in $(1, \dots, N)$ particle **do**
 - 4: $\mathbf{q}_t^i \sim p(\mathbf{q}_t^i | \mathbf{q}_{t-1}^i)$ ▷ State update
 - 5: $\mathbf{w}_t^i \propto p(\mathbf{b}_t | \mathbf{q}_t^i)$ ▷ Weight update
 - 6: $\mathbf{Q}_{t|t} \leftarrow \text{resampling}(\mathbf{Q}_{t|t-1}, \mathbf{w}_t)$
 - 7: $\mathbf{q} \leftarrow \frac{\mathbf{Q}_{t|t}}{N}$
-

The posterior probabilities can be approximated as a set of particles by substituting the weights in Eq. (5).

$$p(\mathbf{q}|\mathbf{b}) = \sum_{k=1}^N \mathbf{w}^k \delta(\mathbf{q} - (\mathbf{q}^k)). \quad (12)$$

Additionally, to summarize the estimation method, we introduce the algorithm shown in Algorithm 1 for estimating the radiation source distribution using a particle filter. First, $\mathbf{Q}_{0|0}$ was scattered appropriately, which is a set of \mathbf{q} of particles by incorporating some prior information. Next, the state of each particle was updated based on the state-update function in each epoch. Because there is no state change between measurements, we added Gaussian noise as the state update function, and even after resampling many times, the final result depended heavily on the initial state. Therefore, by adding Gaussian noise after each epoch, we can reduce the possibility that the estimated value falls into the local maximum:

$$p(\mathbf{q}_t^i | \mathbf{q}_{t-1}^i) = \mathbf{q}_{t-1}^i + \mathcal{N}(\mu, \sigma^2). \quad (13)$$

Next, the likelihood was calculated based on Eq. (10) of each particle whose state has been updated and then derived its weight. Finally, the set of particles $\mathbf{Q}_{t|t}$ was updated using the weights. The radiation source distribution \mathbf{q} is given by the mean of the posterior probabilities $\mathbf{Q}_{t|t}$.

C. Prior Information Based on Structure Information

In the first step of Algorithm 1, when determining the initial particles, it was necessary to set the position and intensity ranges of the particles. We introduced the process of determining the position and intensity ranges of particles using prior information from the survey of the Fukushima Daiichi Nuclear Power Plant Unit 2.

We set the position range to match the size of the hole at the platform at the top of the pedestal. According to the investigation [14] of the top structure and the bottom of the pedestal of Unit 2 at the Fukushima Daiichi Nuclear Power Plant, it was confirmed that the fuel debris dissolved through a part of grating at the pedestal platform, and fell to the pedestal bottom. The gratings and fuel debris mixed together to form clay-like sediments, as shown in Fig. 4, and the sediments appeared to be a solidified molten material. Accordingly, it is conceivable that no deformation occurred after the sediment fell. Furthermore, because cooling water was poured down at the pedestal bottom, and the

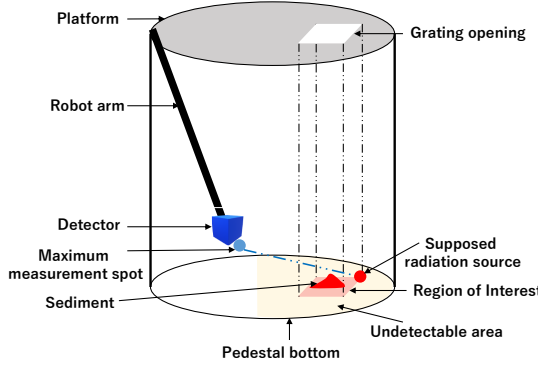


Fig. 4. Measurement system and prior information application

estimated temperature near the bottom of the pedestal was approximately 21°C , the sediment was maintained in a stable cooling state by the cooling water. Therefore, based on the investigation results, we assumed that the radiation sources in the sediment were located just under the opening of the grating, and the possible range in the undetectable area of the radiation sources corresponded to the size of the opening of the grating, and we set the possible range as the region of interest (ROI).

Next, we set the upper limit of the intensity range to the maximum possible intensity of the radiation source, based on the ROI we had determined. As shown in Fig. 4, radiations were measured at the spot closest to the ROI. Based on the measurements, back-calculate the intensity of the assumed radiation source, which is located farthest from the ROI. The intensity was set to the upper limit of the intensity range as for the point-like radiation source. For the distributed radiation source, apply the ROI to the determined grid size, and set the ROI to be filled with the sources in the intensity we back-calculated, and set the intensity of the ROI to the upper limit of the intensity range.

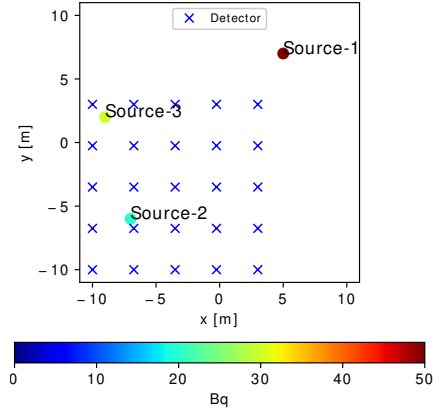
III. SIMULATION SETTINGS AND RESULT

To validate the performance of the particle filter using structural information in an undetectable area, we set the subject to two types of radiation sources: the point-like radiation sources and the distributed radiation sources. At the same time, we compared particle filter and MLE [11], [13] to validate the advantage of the particle filter by incorporating appropriate structure information.

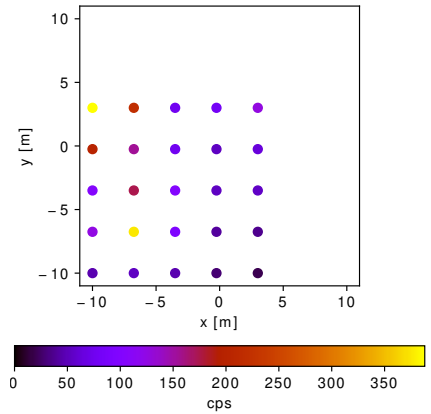
A. Simulation of Point-like Radiation Source

A top view of the bottom of the pedestal is shown in Fig. 5(a), and the size is $10\text{ m} \times 10\text{ m}$, in positions $(5, 7, 0)\text{ m}$, $(-7, -6, 0)\text{ m}$, and $(-9, 2, 0)\text{ m}$, the intensity of 50 Bq, 20 Bq, 30 Bq, three radiation sources were installed. We set the upper right corner of the pedestal as an undetectable area. The detector group was placed at the lower left of the pedestal as the detectable area, and the height was set to 1.5 m. The number of counts measured by the detector is shown in Fig. 5(b).

Next, as the structure information, we assumed that the opening area of the grating was in the center $(5, 7, 3.5)\text{ m}$



(a) Settings of detectors and point-like radiation sources

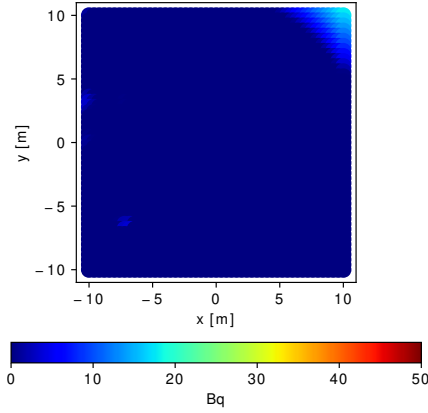


(b) Count number measured from point-like radiation sources

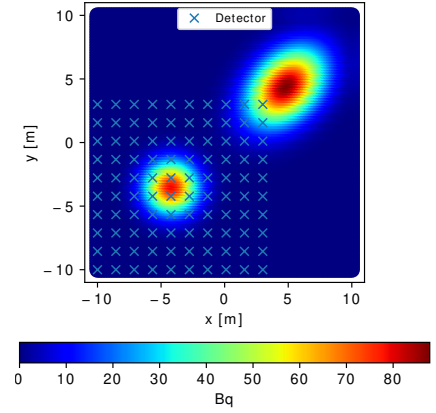
Fig. 5. Simulation settings for point-like radiation sources

and side length 0.6 m. The ROI is the area directly under the opening where the radiation source was likely to be located. Because the opening size was relatively small, we assumed that the radiation source was a point-like source. Then, the upper limit of the intensity range is calculated using the number of counts at the measurement spot $(3, 3, 1.5)\text{ m}$, as shown in Fig. 5(b), which was closest to the ROI. Based on the structural information, we set the number of radiation source candidates at an interval of one to three, and set the possible position of the point-like source in an undetectable area to the area of $x \in [4.7, 5.3]\text{ m}$, $y \in [6.7, 7.3]\text{ m}$, and the intensity π at an interval of 1 to 300 Bq.

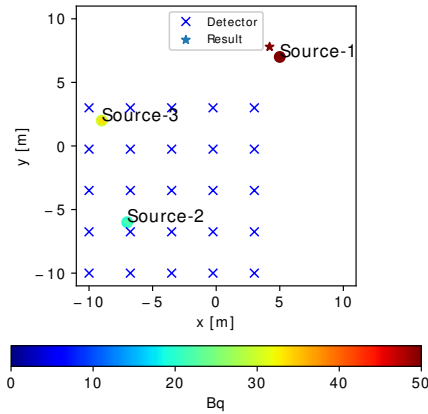
The results estimated by the MLE and the particle filter are shown in Fig. 6(a) and (b), respectively. First, for the MLE, contrasting the number of counts in fig. 5(b), it is clear that the estimation performance strongly depends on the count number distribution, for Source-2 and Source-



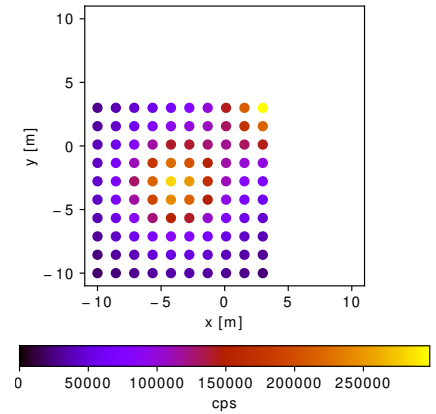
(a) Estimation result of point-like radiation sources by MLE



(a) Settings of detectors and distributed radiation sources



(b) Estimation result of point-like radiation sources by proposed method



(b) Count number measured from distributed radiation sources

Fig. 6. Estimation result of point-like radiation sources

Fig. 7. Simulation settings for distributed radiation sources

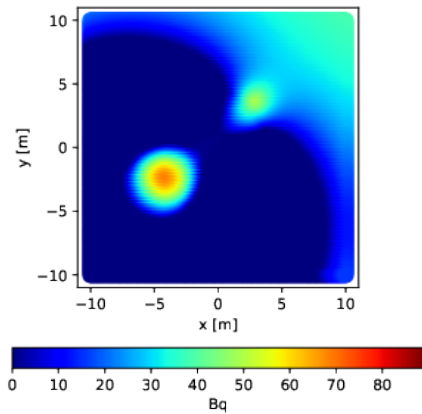
3 at the detectable area, the approximate locations were estimated, but the intensity differed significantly from the ground truth. Source-1, which is in an undetectable area, failed to be estimated. During the estimation of Source-1, the optimization process started from the point with the highest count in the upper right corner, and the arc drawn around the point was clearly visible, indicating a local maximum. On the other hand, the results for the particle filter shown in Fig. 6(b) are almost consistent with the ground truth. As for the point-like radiation source, the performance of the particle filter using the structural information was better than that of the conventional MLE.

B. Simulation of Distributed Radiation Source

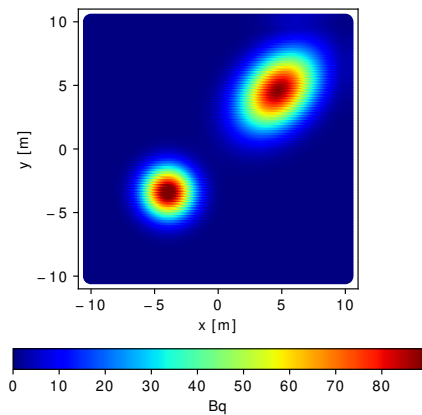
Next, we established two distributed radiation source with a Gaussian distribution: radiation sources in an undetectable area: $\boldsymbol{\mu} = [5, 5]$, $\boldsymbol{\Sigma} = [[4, 2], [2, 4]]$, $q^t = 2000$ Bq, and

radiation sources in a detectable area: $\boldsymbol{\mu} = [-4, -3]$, $\boldsymbol{\Sigma} = [[2, 0], [0, 2]]$, $q^t = 1000$ Bq, as shown in Fig. 7(a). The undetectable and detectable regions were established in the same way as for the point-like radiation source. The number of counts is shown in Fig. 7(b).

As for the structural information, we assumed that the opening area of the grating is in the center (5, 5, 0) m and side length 10 m. The ROI is the area directly under the opening where the radiation source was likely to be located. Because the opening size was relatively large, and the sediment was mountainous and gradually distributed from the center to the periphery, we cannot ignore the distribution of the radiation source, and we supposed that the radiation source followed a Gaussian distribution. Then, the location set $\boldsymbol{\mu} = [\mu_i]$, $\mu_i \in [0, 10]$, $\boldsymbol{\Sigma} = [\Sigma_{ij}]$, $\Sigma_{ij} \in [0, 6]$, $q^t \in [1, 22372]$ Bq was determined.



(a) Estimation result of distributed radiation sources by MLE



(b) Estimation result of distributed radiation sources by proposed method

Fig. 8. Estimation result of distributed radiation sources

The results of the MLE and particle filter estimations are presented in Fig. 8(a) and (b), respectively. Figure 8(a) shows that the MLE method strongly depends on the count number distribution. The estimated results in the detectable area had relatively high accuracy results, which still had an arc around the highest count point in the undetectable area, as same as the point-like radiation source case. This confirmed that the MLE is not capable of estimating radiation sources in an undetectable area. On the other hand, the particle filter, which uses the structural information, showed comparably high accuracy and the potential to be used to estimate radiation sources in an undetectable area.

IV. CONCLUSION

In this study, we targeted the Fukushima Daiichi nuclear disaster and verified that it is possible to estimate the radiation source in an undetectable area using a particle filter by

incorporating structural information. Additionally, the mathematical models we proposed for point-like radiation sources and distributed radiation sources accurately described the relationship between the radiation and the detector, and were applied well to the particle filter. Certainly, the structural information we used is mildly optimistic, and the actual distribution of radiation sources is more complex than what we set. For example, dealing with irregular distributions will be a future issue. We are currently concerned with flow-based density estimation, which can transfer a simple distribution to a complex distribution.

V. ACKNOWLEDGMENT

This work was supported by JAEA Nuclear Energy S&T and Human Resource Development Project.

REFERENCES

- [1] TEPCO. Status of the decommission work. 2020 (Accessed on Oct 20, 2020). <https://www.tepco.co.jp/en/hd/decommission/progress/index-e.html>.
- [2] The picture taken in pcv. 2021 (Accessed on Sep 10, 2021). https://photo.tepco.co.jp/library/180119_01/1_80119_05.jpg.
- [3] Yokoyama R, Kondo M, Suzuki S, Harada M, Okamoto K. Investigation of the outflow and spreading-solidification behaviour of stratified molten metal. *Journal of Nuclear Engineering*. 2021;2(2):168–189. Available from: <https://www.mdpi.com/2673-4362/2/2/17>.
- [4] Cong F, Tamura Y, Shimazoe K, Takahashi H, Ota J, Tong S. Radioactive source recognition with moving compton camera imaging robot using geant4. *Nuclear Instruments and Methods in Physics Research Section A: Accelerators, Spectrometers, Detectors and Associated Equipment*. 2020;953:163108.
- [5] Štibinger P, Báča T, Saska M. Localization of ionizing radiation sources by cooperating micro aerial vehicles with pixel detectors in real-time. *IEEE Robotics and Automation Letters*. 2020;5(2):3634–3641.
- [6] Kim D, Woo H, Ji Y, Tamura Y, Yamashita A, Asama H. 3d radiation imaging using mobile robot equipped with radiation detector. 2017 IEEE/SICE International Symposium on System Integration. 2017;:444–449.
- [7] Cordone G, Brooks RR, Sen S, Rao NS, Wu CQ, Berry ML, Grieme KM. Improved multi-resolution method for mle-based localization of radiation sources. 2017 IEEE 20th International Conference on Information Fusion. 2017;:1–8.
- [8] Deb B, Ross JF, Ivan A, Hartman MJ. Radioactive source estimation using a system of directional and non-directional detectors. *IEEE Transactions on Nuclear Science*. 2011;58(6):3281–3290.
- [9] Gueorguiev A, Preston J, Hoy L, Pausch G, Herbach CM, Stein J. A novel method to determine the directionality of radiation sources with two detectors based on coincidence measurements. *IEEE Nuclear Science Symposium & Medical Imaging Conference*. 2010;:1525–1530.
- [10] Mascarih F, Papachristos C, Wilson T, Alexis K. Distributed radiation field estimation and informative path planning for nuclear environment characterization. 2019 IEEE International Conference on Robotics and Automation. 2019;:2318–2324.
- [11] Morelande M, Ristic B, Gunatilaka A. Detection and parameter estimation of multiple radioactive sources. 2007 IEEE 10th International Conference on Information Fusion. 2007;:1–7.
- [12] Sugaya S, Endo T, Yamamoto A. Inverse estimation methods of unknown radioactive source for fuel debris search. *Annals of Nuclear Energy*. 2019;124:49–57.
- [13] Minamoto G, Takeuchi E, Tadokoro S. Estimation of ground surface radiation sources from dose map measured by moving dosimeter and 3d map. *International Conference on Intelligent Robots and Systems*. 2014;:1889–1895.
- [14] Fukushima daiichi nuclear power station unit 2 primary containment vessel internal investigation results. 2021 (Accessed on Sep 10, 2021). https://www.tepco.co.jp/en/wp-content/uploads/handouts/_190228_01-e.pdf.